NASA
Technical
Paper
2905

1989

Analysis of Nd^{3+}:Glass, Solar-Pumped, High-Power Laser Systems

L. E. Zapata
Miami University
Oxford, Ohio

M. D. Williams
Langley Research Center
Hampton, Virginia

National Aeronautics and
Space Administration
Office of Management
Scientific and Technical
Information Division

Introduction

There is currently much interest in space-based, high-power lasers. Military applications, such as weapons and radars, and civilian applications, such as lidars and the transmission of power to space-based users, would benefit if the primary source of power were plentifully available on-site. In space the only power source for such an activity is solar power. Employing this power, the laser would be self-sufficient, and thus the choice of orbit for the laser would not be bound by the necessity of refueling flights. An additional advantage in efficiency (ref. 1) is realized if the laser medium is *directly* pumped by concentrated sunlight instead of discharges that derive electrical power from solar cells, provided that the laser converts sunlight with a total solar efficiency in the range of 1 to 10 percent. We have analyzed the Nd^{3+}:glass laser medium and found it to be an excellent high-power laser candidate for direct solar-pumping schemes which involve multiple elements and transverse pumping of *slab or fiber lasers* that exploit waveguide principles for the laser optical path. Until now, as we will show, a laser slab would fracture before the threshold solar input would be reached. However, recent breakthroughs in the hardness (refs. 2 and 3) of finished total internal reflection (TIR) laser slabs prompted us to evaluate Nd^{3+}:glass as a direct solar-pumped laser (DSPL).

Both slab and fiber lasers have been proposed in brief in the scientific literature with variations in the material proposed for the medium. Nd^{3+}:YAG fiber bundles were proposed in a Russian paper (ref. 4) that reviewed on broad theoretical grounds all the current gaseous, liquid, and solid solar-pumped (direct and indirect) laser candidates. The Russians concluded that laser fiber bundles would be the most effective solar-pumped lasers, based on total solar efficiency, cooling capacity, and threshold criteria. A Japanese group has reported the highest power recorded to date (18 watts, at 1.6 percent solar efficiency) for an experimental DSPL (ref. 5). They achieved their findings using an Nd^{3+}:YAG rod 4 mm in diameter and 4 cm in gain length pumped by concentrated sunlight at a level of approximately 5000 solar constants (one solar constant equals 0.14 W/cm^2). In their discussion, they also proposed multiple laser elements in series as a means of collecting sunlight more efficiently. The slab geometry was mentioned as well. At Lawrence Livermore National Laboratories (LLNL), multiple slabs are being proposed and fervently being investigated on theoretical and experimental grounds (ref. 6) for the purpose of obtaining pulsed laser beams with very high intensity on the order of (GW/cm^2) with high average power for fusion applications. In contrast to LLNL, because our research is concerned with exploiting solar power in space, we have concentrated on the rather limited, but continuous, solar-pumping power available. The emitted power from the solar surface is 6.3 kW/cm^2 and is the thermodynamic flux limit at the focal spot of an ideal concentrator, providing approximately 46 000 solar constants. Solar-pumped continuous wave (cw) laser beams with relatively low continuous intensity (on the order of kW/cm^2) are possible. Because LLNL and Langley both desire high average power, we are both interested in heat removal and fracture strength of materials. LLNL is well represented in both areas. Their results in strengthening glass laser slabs through special fabrication techniques have resulted in an experimentally tested factor of 12 increase in the rupture strength in ground glass and a factor of 4 increase in the finished laser slabs that were experimentally polished. These special fabrication techniques involve chemical removal of surface cracks introduced during grinding (the major cause of lowered hardness in finished slabs) as an intermediate step between ever-shallower polishing steps (ref. 3). As we will show, hardened slabs can now be made to resist solar-pumping levels above laser threshold, thus permitting multiple slab designs to yield a higher average power.

In what follows we first convoluted the solar power spectrum with the Nd^{3+}:glass absorption bands to find the solar-pumped source term (at one solar constant) for the upper laser level. With this source term, we found the steady state solution to the kinetic equations for this medium in the case of TIR slab laser geometry. We then analyzed the resulting thermal stress as a function of solar-pumping level for any particular design (restricted to TIR slabs) in order to find the range of parameters (in terms of the particular laser glass, slab dimensions, and solar-pumping level) that would produce a usable DSPL device. The trend toward thinner geometries became apparent, and in the Conclusions devices based on multiple slab lasers as well as fiber laser bundles with phase-matched outputs are suggested as means of achieving high average output power.

Symbols

A_{ij}	transition probability, s^{-1}
C	solar concentration factor
c	speed of light, cm/s
cw	continuous wave
E	Young's modulus, N/cm^2

J	surface stress of heat loaded slab, N/cm^2
k	thermal conductivity, (W/cm)/°C
K	stimulated emission coefficient, equal to $\sigma c/n_o$, cm^3/s
ℓ	slab length, cm
N_0	neodymium ion concentration, cm^{-3}
N_1, N_2	lower(1) and upper(2) laser level populations, cm^{-3}
n_0	index of refraction at laser wavelength
Q	heat loading on optically pumped slab, W/cm^3
R_f	fluorescent rate, $cm^{-3}s^{-1}$
R_g	reflectivity of glass-vacuum interface
R_i	intrinsic loss rate, $cm^{-3}s^{-1}$
R_ℓ	laser photon output rate, $cm^{-3}s^{-1}$
R_1, R_2	back and output mirror reflectivities
r_1, r_2	the voltage reflection coefficients for the mirrors, equal to $\sqrt{R_1}$ and $\sqrt{R_2}$, respectively
$S(\lambda)$	flux of solar photons in wavelength interval $d\lambda$, $cm^{-2}s^{-1}$
S_{03}	activation rate of upper vibronic manifold, $cm^{-2}s^{-1}$
S_2	volumetric solar-pumped upper laser level source rate, $cm^{-3}s^{-1}$
t	slab thickness, cm
w	slab width, cm
YAG	yttrium-aluminum-garnet
α	intrinsic loss coefficient, cm^{-1}
α_T	thermal expansion coefficient, $°C^{-1}$
ε	transmissivity of laser glass
η	quantum yield
η_k	kinetic efficiency
λ	wavelength, nm
ν	Poisson's ratio
ρ	laser photon density in single cavity mode, cm^{-3}
σ	stimulated emission cross section, cm^2
$\sigma_a(\lambda)$	Nd^{3+}:glass absorption cross section, cm^2
τ	time, s
τ_c	laser photon cavity lifetime, s
τ_F	fluorescent lifetime, s
τ_{ij}	lifetime for transition from $i \rightarrow j$, s
τ_R	total spontaneous radiative lifetime of upper laser level, s
χ	total power absorbed divided by power that populates the upper laser level
ω	collisional deactivation rate, s^{-1}
Ω	geometrical factor

The Nd^{3+}:Glass Solar-Pumped Laser Model

We have developed a first-order kinetic model that describes the Nd^{3+} laser performance of a solar-energized, face-cooled glass slab. The advantages of a slab configuration are well documented (refs. 7 to 13) and provide the main assumptions for our laser model: the stress-induced birefringence and thermal- and stress-induced focusing can be eliminated by optical propagation along a zigzag path. In addition, the source term is assumed to be distributed homogeneously within the laser volume, which is swept out by a single laser mode summing all cavity modes necessary to fill the gain volume.

The Source Term

Figure 1 illustrates the modeling of the energy level diagram of the Nd^{3+} laser, which is shown in figure 1(a). Due to the random nature of the perturbing micro-environment in the glass host, the Nd^{3+} absorption lines broaden and overlap, resulting in an effective absorption spectrum which is shown (for silicate glass) in figure 2. A total of 35 percent of the solar-power spectrum is encompassed by the absorption bands of figure 2 and represents the limit in collection efficiency that can be achieved—without wavelength shifters (such as dyes) or sensitizers (such as Cr^{3+})—by perfect light traps. Ninety-five percent of the energy absorbed populates the upper manifold which then decays within 20 ns (ref. 14) to the $^4F_{3/2}$

upper laser level as a result of phonon emission. The lifetime of the upper laser level is metastable because of the poor matching with the phonon structure of the host and ranges between 200 and 800 μs depending on the glass host and doping density. The transition with the highest probability is the $^4F_{3/2} \rightarrow {}^4I_{11/2}$ at 1.05 μm. The lower laser level $^4I_{11/2}$ is also phonon terminated and relaxes to the ground state $^4I_{9/2}$ with a lifetime of less than 10 ns (ref. 14). Thus, the kinetics are those of a nearly ideal four-level laser. For the relatively low solar-pumping intensities that are possible, the four-level scheme shown in figure 1(b) can be used. The source term S_{03} is the number of activations into the upper vibrationally relaxed manifold per unit area of absorbing glass and can be found by convolution of the solar spectrum with the absorption coefficient for a given glass thickness and concentration, that is,

$$S_{03} = \int_{325\text{ nm}}^{900\text{ nm}} S(\lambda)\frac{(1-R_g)(1-\varepsilon)}{1-\varepsilon R_g}\,d\lambda \qquad (1)$$

where $\varepsilon = \exp[-N_0\sigma_a(\lambda)t]$.

In equation (1) $S(\lambda)$ is the flux of photons per wavelength interval $d\lambda$ in the solar spectrum at one solar constant incident on the glass slab thickness t, N_0 is the Nd^{3+} doping density, and $\sigma_a(\lambda)$ is the Nd^{3+} absorption cross section as a function of wavelength λ (as shown in fig. 2). The effect of the reflectivity R_g at each glass-vacuum interface has also been included. The integral in equation (1) was evaluated numerically using tabulated values of the solar spectrum and the result, $S_{03}(N_0t)$, is shown as a function of N_0t in figure 3. The upper laser level (ULL) volumetric source term can be calculated as

$$S_2(C, N_0t, t) = \eta C\,\frac{S_{03}(N_0t)}{t} \qquad (2)$$

where the quantum yield η is 0.95, the fraction of activations that relax down to the ULL, $^4F_{3/2}$ and S_2 is the kinetic source term for N_2 per unit volume as a function of the design parameters of doping density N_0, slab thickness t, and solar concentration C.

Rate Equations

Referring to figure 1(b), we write a set of differential equations:

$$\frac{dN_2}{d\tau} = S_2 - K\rho(N_2 - N_1) - \frac{N_2}{\tau_F} \qquad (3)$$

$$\frac{dN_1}{d\tau} = K\rho(N_2 - N_1) + \frac{N_2}{\tau_{21}} - \frac{N_1}{\tau_{10}} \qquad (4)$$

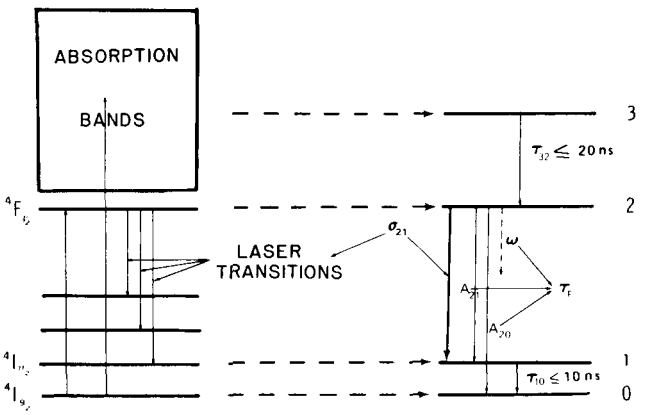

(a) Energy level diagram. (b) Four-level laser.

Figure 1. Modeling of Nd^{3+} energy level diagram.

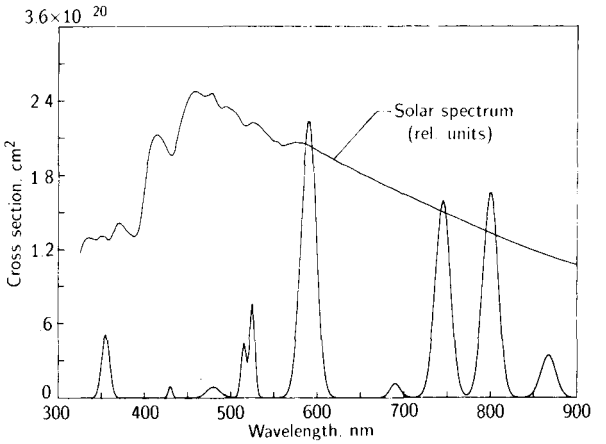

Figure 2. Nd^{3+} absorption spectrum.

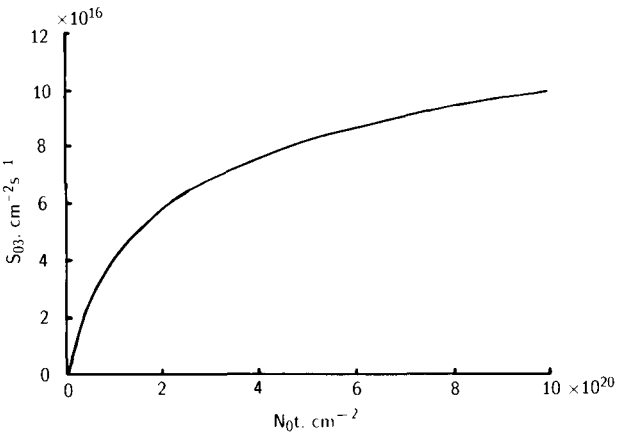

Figure 3. For one solar constant, the number of photons absorbed into the upper manifold S_{03} was numerically computed as a function of the neodymium ion density N_0 times the thickness of the slab t.

$$\frac{d\rho}{d\tau} = K\rho(N_2 - N_1) - \frac{\rho}{\tau_c} + \Omega\frac{N_2}{\tau_{21}} \qquad (5)$$

In equation (3), τ_F is the effective radiative (fluorescent) lifetime of the ULL:

$$\tau_F^{-1} = A_{21} + A_{20} + \omega = \tau_R^{-1} + \omega \qquad (6)$$

where A_{20} is the Einstein coefficient for the ${}^4F_{3/2} \rightarrow {}^4I_{9/2}$ resonance transition and is nearly the same (ref. 14) as A_{21}, the Einstein coefficient for the ${}^4F_{3/2} \rightarrow {}^4I_{11/2}$ laser transition. The effect of concentration quenching and multiphonon relaxation is included in the rate of deactivation due to nonradiative processes ω. The effective lifetime for the ULL can be obtained from experimental fluorescent lifetime measurements (ref. 15).

In equation (5), Ω represents the fraction of spontaneously emitted photons that is confined between the laser mirrors and has a weak influence on threshold. It is of no interest in cw calculations above threshold. In the same equation, the laser photon cavity lifetime τ_c is a function of the intrinsic loss α, the slab length ℓ, and the mirror reflectivities 1 and 2 with its inverse value given as

$$\frac{1}{\tau_c} = \frac{c}{n_0}\left[2\alpha + \frac{1}{\ell}\ln(1/r_1 r_2)\right] \qquad (7)$$

The first factor in brackets represents the loss caused by scattering and absorption of laser radiation by the medium. This varies from host to host but it is nominally less than 0.002 cm^{-1} in glass. The second factor in brackets is the laser photon prorated loss due to the laser output mirror. Any window transmission loss can be lumped in the back mirror reflectivity (r is the dielectric's voltage reflection coefficient: $r = \sqrt{R}$ where R is the reflectivity).

The approximation that $N_1 << N_2$ greatly simplifies the steady state solution of rate equations (3), (4), and (5). The approximation is justified since $\tau_{10} < 10$ ns and the total lifetime τ_2 of the upper laser level is given by

$$\tau_2^{-1} = \tau_F^{-1} + K\rho \qquad (8)$$

The total lifetime shortens from approximately 350 μs (the fluorescent lifetime) at threshold and becomes comparable to τ_{10} at a photon density of the order of 10^{17} photons/cm^3. This photon density corresponds to a laser intensity of 710 MW/cm^2 which is simply unattainable by solar pumping.

The steady state solution to equations (3) and (5) can be found by equating the time derivatives to zero. The algebraic solution becomes

$$\rho = \frac{1}{2}\left[\left(S_2\tau_c - \frac{1}{K\tau_F}\right) + \sqrt{\left(S_2\tau_c - \frac{1}{K\tau_F}\right)^2 + \frac{4\tau_c}{\tau_{21}}\frac{\Omega}{K}S_2}\right] \qquad (9)$$

and

$$N_2 = \frac{S_2}{K\rho + \frac{1}{\tau_F}} \qquad 10)$$

The last term inside the square root in equation (9) is useful in determining threshold and is therefore included in the computer model for this purpose. Above threshold, the ULL population rapidly approaches the value

$$N_{2,\mathrm{th}} = \frac{1}{K\tau_c} \qquad (11)$$

while the photon density continues growing with linear dependence on the source term S_2 approximated by

$$\rho \approx S_2\tau_c - \frac{1}{K\tau_F} \qquad (12)$$

The output mirror reflectivity in equation (7) can be iterated with equation (9) (or (12)) to obtain the maximum (optimum) output power.

Comparison of the Model With Available Experimental Data

In order to ascertain the validity of our first-order kinetic model, two detailed comparisons were made with available experimental data. The first comparison was made with a solar-pumped cw 18-watt Nd:YAG rod laser (ref. 5), and the second with the reported performance of a slab-geometry Nd:glass laser (ref. 10).

From available Nd:YAG laser data, the material parameters, such as stimulated emission cross section, intrinsic loss cm^{-1}, fluorescent lifetime, and doping density, were input to the model. The gain length, output mirror transmission, and solar concentration ($C \approx 5000$ solar constants) were taken from reference 5 and the cw output power computed at 20 watts, 1.61-percent total efficiency—in very good agreement with the 18 watt, 1.6 percent reported. We calculated (from the results presented in the section entitled "Thermal Stress Limit") that the rod was operated at a factor of 28 from its fracture limit.

Because thick slabs are not capable of withstanding the cw heat load necessary to reach threshold, presently there are no data on cw Nd:glass laser slabs.

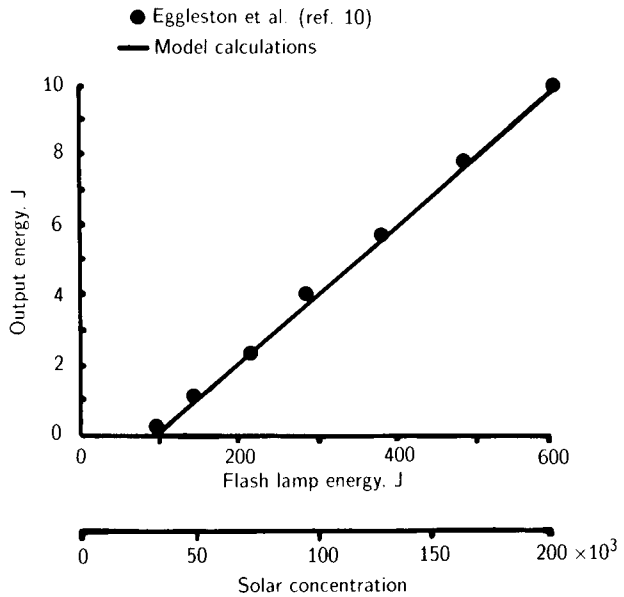

Figure 4. Comparison of experimental data with our own modeling computations for cw Nd^{3+}:glass laser.

We have therefore compared the above model with the pulsed Nd:glass laser slab tested by Eggleston et al. (ref. 10). The pulse length of 170 μs is much longer than the $\approx$ 30-μs total effective lifetime of the upper laser level at the estimated peak concentration (solar equivalent) of 200 000 suns; thus the cw laser analysis is valid and need only be truncated to accommodate the appropriate pumping time. From data for the 2200 A/cm^2 lamps used in the experiment the equivalent solar concentration was calculated by assuming a 38-percent electrical-to-spectral lamp output efficiency, with a further assumption of 85-percent reflection for the reflector structure and a 15-percent absorption per pass by the slab. The agreement (see fig. 4) is nearly perfect throughout the operation range reported.

The Nd^{3+} laser model used is therefore accurate and helpful in determining scaling trends for a given material.

Kinetic Efficiency Computations

Once a solar photon has been absorbed into the upper level manifold, it will populate the upper laser level $^4F_{3/2}$ with a 95-percent quantum yield. The upper level's fluorescent lifetime τ_F is sensitive to concentration quenching, which is strongest in silicates and constitutes an important loss mechanism. Graphical data compiled by SCHOTT (ref. 15) on τ_F for laser glasses were fitted with a second-order equation and used in our modeling computations for optimizing the Nd^{3+} concentration for the several laser materials we have investigated.

Within a fluorescent lifetime τ_F, the upper laser level emits a laser or a fluorescent photon. There is only one source of fluorescent photons:

$$R_f = \frac{N_2}{\tau_F} \qquad (\mathrm{cm^{-3}s^{-1}}) \tag{13}$$

For our purpose, we consider that all fluorescent photons escape the medium. Two mechanisms exist that remove laser photons; both are found in the expression for the laser photon cavity lifetime (eq. (7)). These two mechanisms are due to the intrinsic loss in the host medium and to the laser photon output rate at the output mirror:

$$R_i = \frac{2\rho c}{n_0}\,\alpha \qquad (\mathrm{cm^{-3}s^{-1}}) \tag{14}$$

$$R_\ell = \frac{\rho c}{n_0 \ell}\ln(1/r_1 r_2) \qquad (\mathrm{cm^{-3}s^{-1}}) \tag{15}$$

The kinetic (or internal conversion) efficiency of solar-activated upper laser levels to output laser photons is given by R_ℓ/S_2, that is,

$$\eta_k = \frac{c\ln(1/r_1 r_2)}{n_0 \ell}\frac{\rho}{S_2} \tag{16}$$

If equation (7) is used in equation (16), we obtain values above threshold, that is, in the regime of equations (11) and (12):

$$\eta_k = \left(1 - \frac{N_{2,\mathrm{th}}}{S_2 \tau_F}\right) \Big/ \left[1 + \frac{2\alpha\ell}{\ln(1/r_1 r_2)}\right] \tag{17}$$

The strongest driver in the above equation is the source term S_2. As S_2 increases, the output mirror reflectivity decreases (for maximum power optimization) making the denominator smaller while making the numerator larger. The kinetic efficiency therefore asymptotically approaches a maximum found at high solar concentrations.

We have taken the kinetic efficiency as the figure of merit for the materials studied because the total solar efficiency is influenced by the design of the light trap surrounding the slab laser. If the pumping radiation were allowed two passes through the slab laser, the source term and therefore the internal efficiency as well as the total efficiency would increase markedly. For example, a slab, 2 mm × 1 cm × 15 cm, operates at the rupture limit to produce laser output of 330 watts. If only one pass is allowed for the pumping radiation, this slab requires 14 780 solar constants and converts 1.07 percent of the solar power incident. For two passes, 9320 solar constants convert at 2.15 percent total efficiency. However, all the calculations that follow assume a single pass.

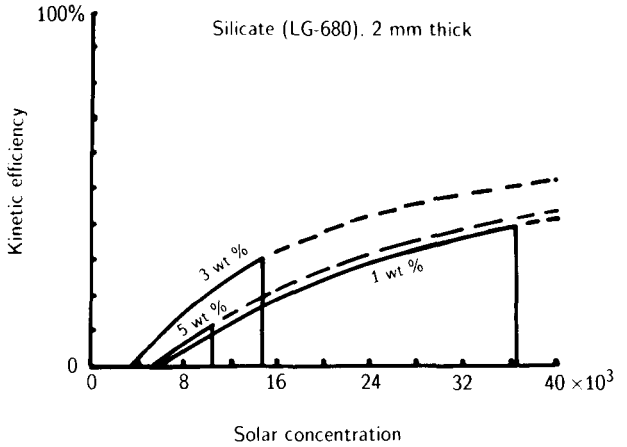

Figure 5. The internal kinetic efficiency vs. solar concentration is shown for three doping densities of the neodymium ion. Due to concentration quenching, this efficiency is optimized at about 3 wt percent.

A sample run for the selection of Nd_2O_3 doping density is shown in figure 5. At all possible solar irradiation levels, 3-percent Nd_2O_3 by weight optimizes the internal conversion efficiency for the 2-mm thick silicate slab (SCHOTT LG-680). Lower doping decreases the source term, while higher doping produces losses through concentration quenching.

The optimized Nd_2O_3 doping was similarly found for the phosphate glasses LG-750 (6 percent) and LG-760 (8 percent). In phosphate glasses, the upper level lifetime is less sensitive to concentration quenching; thus we calculated the higher doping levels. For Nd^{3+}:YAG, atomic 1 percent is presently the available standard.

Thermal Stress Limit

Once the design parameters for a laser slab are chosen (σ, n_0, ℓ, N_0t, t, w), the source term can be calculated as a function of the incident solar concentration C. The heat evolved per unit volume Q, can be calculated from the source term S_2. Every solar photon of average energy $\overline{h\nu}(3.2 \times 10^{19}$ joule) absorbed will convert half of this energy to heat and the rest to either fluorescent or laser photons. Additional heat energy may evolve due to the glass host ultraviolet and infrared absorption bands. The factor χ depends mainly on spectral filtering and varies between 1 and 2. Thus,

$$Q(C) = \left(\frac{\chi}{\chi + 1}\right) \overline{h\nu} S_2(C) \qquad (\mathrm{W/cm^3}) \qquad (18)$$

We have chosen $\chi = 1$ which would be the optimum (minimum) heat evolved for a real device.

The surface stress generated by optical pumping in a uniformly pumped, face-cooled slab at steady state is related to the thermal power per unit volume $Q(C)$ and is given by the equation (ref. 12)

$$J = \left[\frac{\alpha_T E}{3k(1-\nu)}\right] Qt^2 \qquad (19)$$

The factor in brackets is a constant of the material parameters while J has a practical limit $J_{\max}$ that depends on the surface quality of the finished slab.

Because it depends strongly on the surface quality and preparation procedures, the fracture limit $J_{\max}$ is not well determined and consequently is known for only a few materials. It has been shown experimentally (ref. 2) that for polished silicate glass the mean fracture strength increases by a factor of 12 after a 30-minute etch in 5-percent HF. Hulme and Jones (ref. 12) report that in tests with laser slabs, the maximum operating heat load is approximately 30 percent of the fracture stress limit. Hulme and Jones then give graphical information relating the heat load Q to the slab thickness at the fracture limit, which can be fitted by the expression:

$$Qt^2 = 3.6 \qquad (\mathrm{W/cm}) \qquad (20)$$

which carries implicitly all the material constants and $J_{\max}$ in equation (19). We can now solve for $J_{\max}$, which is found to be 1.1 $\mathrm{N/cm^2}$.

As a cross-check, Eggleston et al. (ref. 10) report that their 0.83-cm-thick slab ruptures at a heat loading of 4 $\mathrm{W/cm^3}$. Thus the product $Qt^2 = 2.8$ is close to that given by equation (20). In our calculations, we have been cautious believers of the chemical etch procedure developed at LLNL (ref. 2), and as a consequence, we increased the hardness by a factor of approximately 4 (rather than 12). That is, the slab will not fracture as long as

$$Qt^2 \leq 12 \qquad (\mathrm{W/cm}) \qquad (21)$$

with the equality representing the limit in fracture strength of the material. By using equation (18) and the design parameter t in equation (21), we can determine the limits of solar concentration C on any slab laser material and design that we choose. We note, however, that even a factor of 4 increase in fracture strength falls short by a factor of 20 of the limit reported in reference 16.

Results

We have compared the internal kinetic efficiency for the silicate glass LG-680, the phosphate glasses LG-750 and LG-760, and Nd^{3+}:YAG as a function of input solar concentration. The results are given in graphic form in figure 6 for 5-mm-, 2-mm-, and

1-mm-thick slabs. The rupture limit is represented by the vertical line that meets the internal efficiency curve for the material. The same value for the constant in equation (21) was used for the phosphate and the silicate glasses, the same rupture parameter being assumed for both types of glasses. The rupture parameter used for YAG was 4 times higher than that used for glass (ref. 17). As seen in figure 6, all 5-mm-thick slabs investigated except YAG will rupture before threshold is reached; however, the situation improves markedly for glass as the slabs become thinner. A 1-mm × 1-cm × 15-cm LG-760 phosphate slab is predicted to operate at 23 800 solar constants (the rupture limit) for a single pass, with a total solar efficiency of 3.13 percent producing 1560 watts of useful laser output. Light trapping or dyes would boost the total efficiency while decreasing the solar concentration required.

The YAG offers the best internal efficiency and can withstand the highest solar inputs; however, the production cost for YAG is very high and only limited sizes are possible. This is not the case for glass, which is inexpensive and can be produced in much larger sizes. A more feasible solar-pumped laser may be a mosaic of small slabs made of LG-760 phosphate glass, 2 mm in thickness and 200 cm on each side. When irradiated at 6300 solar constants (rupture limit 7700), the slabs would produce 1 MW of laser power at 2.9-percent total solar efficiency. While presently this size is not an industry standard, there are not, at least at first glance, any insurmountable engineering problems; the most precarious might be the alignment of the segments to optical flatness specifications and the index matching at the interfaces of the multiple slabs. Should this be the case, a possible solution might be to phase-match several beams to produce the desired output.

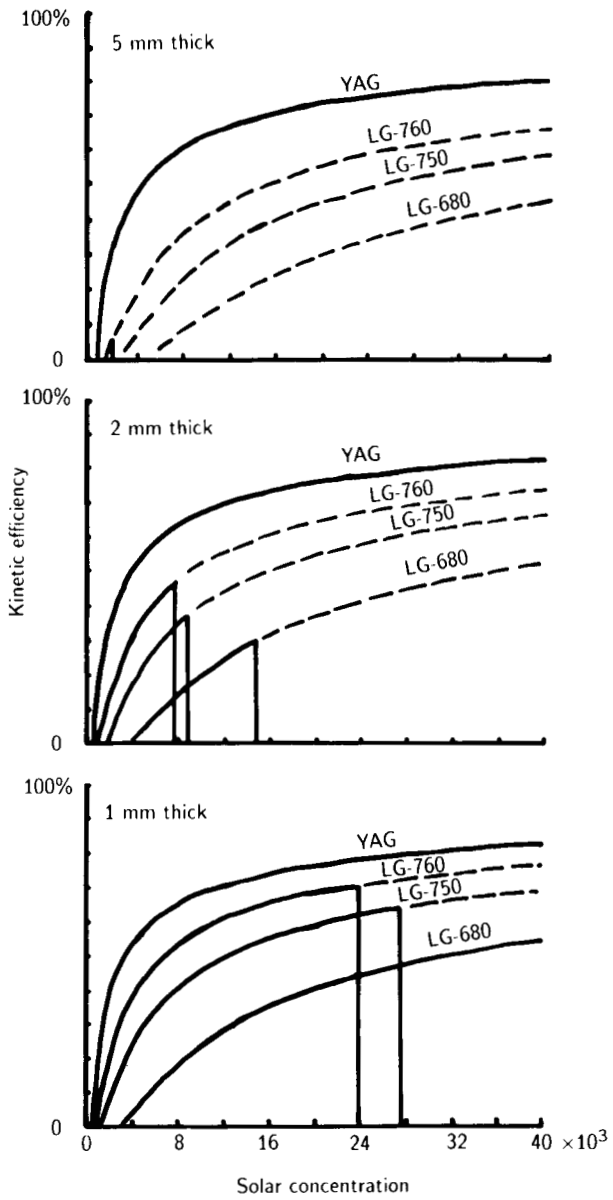

Figure 6. Calculated internal conversion (kinetic) efficiency for Nd^{3+}:YAG, phosphate glasses (LG-750 and LG-760), and silicate glass (LG-680) as a function of solar concentration factor for the thicknesses indicated. Thinner slabs can withstand higher pumping levels and are therefore more efficient.

Novel Approaches to Nd^{3+}:Glass Solar-Pumped Lasers

The Multi-Slab Laser

The above analysis shows that for the slab geometry and zigzag laser beam propagation in particular, a solar-pumped laser becomes possible and more efficient (internally) as the slab becomes thinner. A practical 1-MW solar-pumped laser was suggested utilizing a 4-m^2 mosaic slab, 2 mm in thickness. In fact, as can be seen from equation (21), a factor of 2 reduction in thickness allows for a factor of 4 increase in specific power loading capability.

The disadvantage of thinner slabs is that they absorb less sunlight per pass. This means that the total solar efficiency remains at a few percent even when the internal kinetic efficiency allows tens of percent of the absorbed power to be converted to laser power. Absorption efficiency by thin slabs can be improved by a geometrical arrangement that permits each beam of sunlight multiple passes through the gain medium. While the mosaic large slab design provides an effective solution for the thermal and optical problems, there are other solutions that come to

mind that exploit thinness (for high heat load capability) and optical paths of folded symmetry.

Nd^{3+} Glass Fiber Bundle Array Laser

There is no doubt that fiber optic technology has matured. The production of Nd^{3+} doped glass fibers would seem straightforward in itself since all that is required is that Nd_2O_3 be added to the melt. In fact, there has been a continuous glass laser in existence since 1963, based on this concept (ref. 18). The modes are propagated within the fiber core and folded symmetrically about the central axis; thus the stress- and thermal-induced focusing becomes negligible. If thin fibers were used (10 μm), only a single mode of diffraction-limited waist would propagate. At the output, the expanding beam could be fed into a telescopic mirror for long-range transmission. Even at the highest solar concentrations the thermal stress would be minimal for these fibers. Fiber bundles and light traps can be envisioned. There have been two recent Russian publications which report lasing in Nd^{3+}:silicate glass fibers, 40 μm in diameter and 40 to 150 cm long (ref. 19), and in Nd^{3+}:silicate glass needle rods, 1 mm in diameter and 40 cm long (ref. 20). Both devices lased quasi-cw by internal reflection. The needle rods also lased longitudinally. The needle rods reportedly produced 10^2 to 10^3 times as much power as the fibers. Color centers induced by the ultraviolet component of their flash lamps caused self Q-switching above a certain threshold input producing, in both the fibers and the needle rods, giant laser pulses tens of nanoseconds long that repeated every few tens of microsecond.

It seems feasible to immerse a bundle of these fibers (or needles) in a flowing liquid coolant and to provide feedback to the internally propagating modes in order to obtain phase-matched output as is now done with diode arrays. Another approach is to immerse the fibers (or needle lasers) in an index-matched coolant and arrange them in an array that would tailor the gain profile so that a longitudinal Gaussian laser mode might be exploited.

Conclusions

The principal motivation for this study was the need to evaluate the Nd^{3+} laser as a possible choice for a high-power, space-based laser. Other space-based lasers are being proposed and certainly some of them are at a more mature stage of development than our model (such as the U.S. Air Force's chemical lasers). However, the main advantage of the solid-state media proposed here is that the solar-pumped laser need not be refueled because sunlight, its primary source of power, is available on-site.

We must point out that if the Nd^{3+} host medium were YAG (an even more promising crystal is Cr^{3+}:Nd^{3+}:GdScGa-garnet (ref. 21)),the high-power, solar-pumped laser is presently possible. Nd^{3+}:YAG laser slabs have already produced average powers as high as 400 watts and several industrial groups are now experimenting with kilowatt slabs. For the moment, the maximum possible size for each YAG slab is approximately $20 \times 2.5 \times 0.5$ cm at a cost of \$20 000. One can easily envision a mosaic of 1000 of these slabs, producing 1 MW of power. Using YAG, our calculations show that an 80- $\times$ 80-cm mosaic (containing 128 of the above slabs) would produce 1 MW of laser power at a solar concentration of 40 000 with a 3.5-percent conversion efficiency.

The Nd^{3+}:glass fiber is also a very plausible candidate for a high-power, solar-pumped laser. We do not anticipate problems in cooling. Single mode fibers propagate a single mode which is already at its minimum waist diameter and the diffraction is kept balanced by the refraction of the index gradient (or step in index). Therefore, the beam obtained is a single mode, Gaussian profile, ideally suited for long-range transmission. How the multiple output beams would be summed or whether they would need to be phase-matched needs to be addressed; however, the outlook is promising.

High-power, solar-pumped lasers based on Nd^{3+}:solid-state host are possible today if YAG is used as the host medium. A very promising outlook was also found for hardened glass hosts, when the laser is fashioned into the slab zigzag geometry, and for Nd doped optical fibers.

NASA Langley Research Center
Hampton, VA 23665-5225
April 15, 1986

References

1. Holloway, Paul F.; and Garrett, L. Bernard: Utility of and Technology for a Space Central Power Station. AIAA-81-0449, Feb. 1981.
2. Marion, John E.: Fracture of Solid State Laser Slabs. *J. Appl. Phys.*, vol. 60, no. 1, July 1, 1986, pp. 69–77.
3. Marion, J.: Strengthened Solid-State Laser Materials. *Appl. Phys. Lett.*, vol. 47, no. 7, Oct. 1, 1985, pp. 694–696.
4. Golger, A. L.; and Klimovskii, I. I.: Lasers Pumped by Solar Radiation (Review). *Soviet J. Quantum Electron.*, vol. 14, no. 2, Feb. 1984, pp. 164-179.
5. Arashi, Haruo; Oka, Yasuo; Sasahara, Nenokichi; Kaimai, Atsushi; and Ishigame, Mareo: A Solar-Pumped cw 18 W Nd:YAG Laser. *Japanese J. Appl. Phys.*, vol. 23, no. 8, Aug. 1984, pp. 1051–1053.

6. Emmett, J. L.; Krupke, W. F.; and Sooy, W. R.: *The Potential of High-Average-Power Solid State Lasers.* UCRL 53571, Lawrence Livermore Nat. Labs., Univ. of California, Sept. 1984.
7. Eggleston, J. M.; Kane, T. J.; Kuhn, K.; Unternahrer, J.; and Byer, R. L.: The Slab Geometry Laser—Part I: Theory. *IEEE J. Quantum Electron.*, vol. QE-20, no. 3, Mar. 1984, pp. 289–301.
8. Kane, Thomas J.; Eggleston, John M.; and Byer, Robert L.: The Slab Geometry Laser—Part II: Thermal Effects in a Finite Slab. *IEEE J. Quantum Electron.*, vol. QE-21, no. 8, Aug. 1985, pp. 1195–1210.
9. Eggleston, John Marshall, III: Theoretical and Experimental Studies of Slab Geometry Lasers. Ph.D. Diss., Stanford Univ., 1983.
10. Eggleston, J. M.; Kane, T. J.; Unternahrer, J.; and Byer, R. L.: Slab-Geometry Nd:Glass Laser Performance Studies. *Opt. Lett.*, vol. 7, no. 9, Sept. 1982, pp. 405–407.
11. Chernoch, Joseph P.: *High Power Nd:YAG Mini-FPL.* AFAL-TR-75-93, U.S. Air Force, July 1975. (Available from DTIC as AD A012 579.)
12. Hulme, G. J.; and Jones, W. B.: Total Internal Reflection Face Pumped Laser: Concept and Design Consideration. *Optical Design Problems in Laser Systems, Volume 69 of Proceedings of the Society of Photo-Optical Instrumentation Engineers*, Walter R. Sooy, ed., 1975, pp. 38-44.
13. Jones, William B., Jr.: *Face-Pumped Laser With Diffraction-Limited Output Beam.* U.S. Patent 4,214,216, July 1980.
14. Brown, David C.: *High-Peak-Power Nd:Glass Laser Systems.* Springer-Verlag Berlin Heidelberg New York, 1981.
15. SCHOTT Laser Glass. *Modern Glass Technology for Peak Performance.* SCHOTT Glass Technologies Inc.
16. Levi, Leo: *Applied Optics—A Guide to Optical System Design/Volume 2.* John Wiley & Sons, Inc., c.1980.
17. Marion, John E.: Strengthening of Solid-State Laser Materials. *Conference on Lasers and Electro-Optics—Digest of Technical Papers*, Optical Society of America and Institute of Electrical and Electronic Engineers, c.1985, p. 232.
18. Young, C. G.: Continuous Glass Laser. *Appl. Phys. Lett.*, vol. 2, no. 8, Apr. 15, 1963, pp. 151–152.
19. Dzhibladze, M. I.; Teplitskii, É. Sh.; and Érikashvili, R. R.: Regenerative Glass-Fiber Neodymium Quantum Amplifier. *Soviet J. Quantum Electron.*, vol. 14, no. 1, Jan. 1984, pp. 85 88.
20. Dzhibladze, M. I.; Lazarev, L. E.; and Mshvelidze, G. G.: Stimulated Emission From a Needle-Shaped Neodymium Glass Laser. *Soviet J. Quantum Electron.*, vol. 14, no. 1, Jan. 1984, pp. 89–91.
21. Pruss, D.; Huber, G.; Beimowski, A.; Laptev, V. V.; Shcherbakov, I. A.; and Zharikov, Y. V.: Efficient Cr^{3+} Sensitized Nd^{3+}:GdScGa-Garnet Laser at 1.06 μm. *Appl. Phys. B*, vol. 28, no. 4, Aug. 1982, pp. 355–358.

NASA
National Aeronautics and Space Administration

Report Documentation Page

1. Report No.	2. Government Accession No.	3. Recipient's Catalog No.
NASA TP-2905		

4. Title and Subtitle	5. Report Date
Analysis of Nd^{3+}:Glass, Solar-Pumped, High-Power Laser Systems	February 1989
	6. Performing Organization Code
7. Author(s)	8. Performing Organization Report No.
L. E. Zapata and M. D. Williams	L-16085
9. Performing Organization Name and Address	10. Work Unit No.
NASA Langley Research Center Hampton, VA 23665-5225	506-41-41-01
	11. Contract or Grant No.
12. Sponsoring Agency Name and Address	13. Type of Report and Period Covered
National Aeronautics and Space Administration Washington, DC 20546-0001	Technical Paper
	14. Sponsoring Agency Code

15. Supplementary Notes

16. Abstract

The operating characteristics of Nd^{3+}:glass lasers energized by a solar concentrator were analyzed for the hosts YAG, silicate glass, and phosphate glass. The modeling is based on the slab zigzag laser geometry and assumes that chemical hardening methods for glass are successful in increasing glass hardness by a factor of 4. On this basis, it was found that a realistic 1-MW solar-pumped laser might be constructed from phosphate glass 4 m^2 in area and 2 mm in thickness. If YAG were the host medium, a 1-MW solar-pumped laser need only be 0.5 m^2 in area and 0.5 cm in thickness, which is already possible. In addition, Nd^{3+} doped glass fibers were found to be excellent solar-pumped laser candidates. The small diameter of fibers eliminates thermal stress problems, and if their diameter is kept small (10 μm), they propagate a Gaussian single mode which can be expanded and transmitted long distances in space. Fiber lasers could then be used for communications in space or could be bundled and the individual beams summed or phase-matched for high-power operation.

17. Key Words (Suggested by Authors(s))	18. Distribution Statement
Solar-pumped Nd^{3+}:glass laser Waveguide Nd^{3+} laser	Unclassified—Unlimited Subject Category 36

19. Security Classif.(of this report)	20. Security Classif.(of this page)	21. No. of Pages	22. Price
Unclassified	Unclassified	10	A02

NASA FORM 1626 OCT 86

NASA-Langley, 1989

For sale by the National Technical Information Service, Springfield, Virginia 22161-2171